Revisiting western United States hydroclimate during the last deglaciation

Minmin Fu[1]

[1]Yale University

December 7, 2022

Abstract

During the last ice age, the western United States was covered by large lakes, sustained partly by higher levels of precipitation. Increased rainfall was driven by the atmospheric circulation associated with the presence of large North American ice sheets, yet Pleistocene lakes generally reached their highstands not at glacial maximum but during deglaciation. Prior modeling studies, however, showed nearly monotonic drying since the last glacial maximum. Here I show that iTraCE, a transient climate simulation of the last deglaciation, run at higher resolution and with updated boundary conditions, reproduces a robust peak in winter rainfall over the Great Basin near 16 ka. I further demonstrate that the simulated peak is driven by a transient southward shift of the midlatitude jet. The causes for the southward shift of the jet are multifactorial, with meltwater forcing, changing orbital conditions, and rising atmospheric CO2 all playing a role.

Revisiting western United States hydroclimate during the last deglaciation

Minmin Fu[1]

[1]Department of Earth and Planetary Sciences, Yale University, New Haven, CT, USA

Key Points:

- Geological evidence indicates many lakes over the western United States reached their highstands during the last deglaciation.
- iTraCE, a transient simulation of the last deglaciation, shows wetter conditions at 16 ka than at 20 ka and compares well to proxy evidence.
- Meltwater flux, orbital conditions, and rising atmospheric CO_2 all contribute to lake expansions inferred during Heinrich Stadial 1.

Corresponding author: Minmin Fu, `minmin.fu@yale.edu`

Abstract

During the last ice age, the western United States was covered by large lakes, sustained partly by higher levels of precipitation. Increased rainfall was driven by the atmospheric circulation associated with the presence of large North American ice sheets, yet Pleistocene lakes generally reached their highstands not at glacial maximum but during deglaciation. Prior modeling studies, however, showed nearly monotonic drying since the last glacial maximum. Here I show that iTraCE, a transient climate simulation of the last deglaciation, run at higher resolution and with updated boundary conditions, reproduces a robust peak in winter rainfall over the Great Basin near 16 ka. I further demonstrate that the simulated peak is driven by a transient southward shift of the midlatitude jet. The causes for the southward shift of the jet are multifactorial, with meltwater forcing, changing orbital conditions, and rising atmospheric CO_2 all playing a role.

Plain Language Summary

At the height of the last ice age, the western United States was covered by large lakes such as Lake Bonneville and Lake Lahontan that required more rainfall to be sustained. It is believed that the three to four kilometer thick North American ice sheet over Canada acted as an obstacle to the atmospheric flow, forcing storms to be deflected southward over the Southwestern US, hence bringing more winter rain. Yet if the presence of the ice sheet is responsible for bringing extra rainfall to the western US, why does geological evidence indicate that most lakes attained their maximum size not when the ice sheet was at it largest, but rather when the ice sheet was already melting? Here, I use a climate simulation to show that changes to Earth's tilt and temperature, in conjunction with changes in ocean circulation, caused a temporary increase in rainfall that later reversed when the ice sheet started to retreat more rapidly.

1 Introduction

The hydrological cycle over the western United States has varied dramatically in past climates (Ibarra et al., 2018). During the Last Glacial Maximum (LGM; $\sim$ 20 ka), much of western North America was covered in large lakes, reflecting increased precipitation and reduced potential evapotranspiration (Hostetler & Benson, 1990; Ibarra et al., 2014; Tabor et al., 2021). The Great Basin, the largest closed watershed over North America, is arid in the modern climate, yet was characterized by expansive lakes such as Lake Lahontan and Lake Bonneville during the last glacial period (Broecker & Orr, 1958; Mifflin & Wheat, 1979; Reheis et al., 2014). Multiple lines of geological evidence suggest that much of the southwest US was wetter during the LGM, albeit with a dipole structure characterized by more-arid-than-present conditions over northwestern North America (Oster et al., 2015).

Previous studies have sought to identify the mechanism by which more rainfall was supplied to the Great Basin during the LGM (Kageyama et al., 2021). One hypothesis is that the Cordilleran and Laurentide ice sheets acted as a topographic obstacle that split or diverted the jet stream, leading to a southward deflection of midlatitude storms (COHMAP Members, 1988; Kutzbach & Wright Jr, 1985; Lora et al., 2017; Manabe & Broccoli, 1985). Other suggestions include moisture transport from the south (Lyle et al., 2012), ice-sheet albedo (Bhattacharya et al., 2017), or the presence of a midlatitude waveguide (Lofverstrom, 2020). A recent study showed that mechanical forcing alone may be insufficient and that atmosphere-ocean feedbacks play a role as well (Amaya et al., 2022). Although the detailed mechanisms of the atmospheric response continue to be debated, the presence of the Cordilleran and Laurentide ice sheets led to a major reconfiguration of the hydrological cycle over the western United States with topography, albedo, and air-sea fluxes all playing a role.

Modeling studies generally reproduce wetter conditions over the western US during the LGM (Brady et al., 2013; Kutzbach & Wright Jr, 1985; Lora et al., 2017; Scheff et al., 2017). However, a more subtle feature of the hydrological cycle during glacial periods is that lake highstands over the western US were generally achieved during the last *deglaciation*, and not during the LGM (Lyle et al., 2012). In the Great Basin, lake highstands at most sites occurred around Heinrich Stadial 1 (HS1; ∼18 to 14.7 ka; Munroe & Laabs, 2013b; Reheis et al., 2014). In contrast to the geological record, a previous modeling study involving transient simulation of climate over the last 21,000 years (TraCE-21ka; Liu et al., 2009) showed near-monotonic drying over the western US following the LGM (Lora & Ibarra, 2019), whereas increased precipitation is necessary to explain inferred lake expansions (McGee et al., 2018). Figure 1 shows maximum lake extents during the last deglaciation as well as a compilation of various basins and their highstand ages.

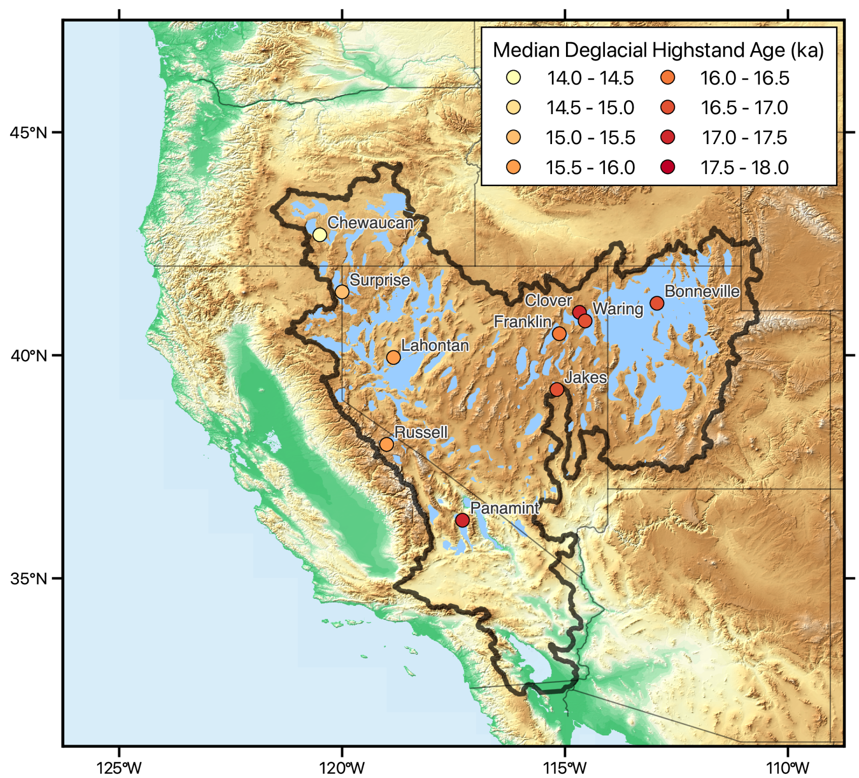

Figure 1. Topographic map of the western United States, showing the maximum extent of pluvial lakes during the last deglaciation (Mifflin & Wheat, 1979) and the median timing of deglacial highstands. The black curve outlines the Great Basin watershed boundary. Approximate age of deglacial lake highstands shown for Lake Bonneville (18–16 ka; McGee et al., 2012; Oviatt, 2015), Chewaucan Basin (14.2±0.2 to 14.6±0.3 ka; Hudson et al., 2017), Clover Basin (17.3±0.2 ka; Munroe & Laabs, 2013b), Franklin Basin (15.8±0.2 to 16.4±0.2 ka; Munroe & Laabs, 2013a), Lake Waring (16.6±0.4 ka; Munroe & Laabs, 2013b; García & Stokes, 2006), Jakes Basin (16.8±0.2 ka; García & Stokes, 2006), Lahontan Basin (15.7±0.2 ka; Adams & Wesnousky, 1998), Lake Russell (15.7±0.2 ka; Benson et al., 1998), Panamint Basin (17.0±0.3 to 17.2±0.3 ka; Jayko et al., 2008), and Surprise Basin (15.2±0.2; Ibarra et al., 2014). Figure and data compilation adapted from McGee et al. (2018).

Here, I investigate the cause of western US lake expansions during the last deglaciation using the isotope-enabled transient climate experiment (iTraCE), a transient simulation of the last deglaciation. Whereas TraCE-21ka, a previous simulation run using an older and coarser climate model, showed nearly monotonic drying since the LGM (Lora et al., 2016; Lora & Ibarra, 2019), iTraCE reproduces a robust peak in winter rainfall over the Great Basin watershed at $\sim$16 ka. By utilizing the "stacked forcing" experiments offered by iTraCE, where four major forcing factors (ice sheet boundary conditions, insolation forcing, greenhouse gases, and meltwater fluxes) are applied additively, I quantify the contributions of these factors to the prominent peak in rainfall seen at $\sim$16 ka.

In Section 2, I introduce my methodology, including details about the iTraCE simulation and its boundary conditions. Section 3 describes my results, including analysis of the western US hydrological cycle, North Pacific atmospheric circulation, and their sensitivity to meltwater fluxes, insolation, atmospheric CO_2, and other forcings. I conclude and discuss implications of the results in Section 4.

2 Methods

This study utilizes iTraCE, the isotope-enabled transient climate experiment, a simulation of the last deglaciation from 20 to 11 ka. iTRACE is performed with the isotope enabled version of the Community Earth System Model version 1.3 (iCESM1.3; Brady et al., 2019) and compares favorably to Greenland ice core oxygen isotope δ18O records (He et al., 2021a) and speleothem records of Asian monsoon rainfall (He et al., 2021b). Key differences between TraCE-21ka (Liu et al., 2009) and iTraCE include an update of the climate model from CCSM3 to iCESM1.3, whereby the atmospheric component changed from the Community Atmosphere Model version 3 (CAM3) to version 5.3 (iCAM5.3). Additionally, ice sheet boundary conditions were updated from ICE-5G (Peltier, 2004) to ICE-6G (Peltier et al., 2015), and iTraCE is run at finer $\sim$2° horizontal resolution rather than the coarser 3.75° resolution of TraCE-21ka. Ice sheet topography (Peltier et al., 2015) and deglacial CO_2 (Lüthi et al., 2008; Monnin et al., 2001) are shown in Supplementary Information Figs. S1,S2.

To allow for the separation of individual forcing factors, iTraCE includes simulations with major forcing factors applied additively. Starting with LGM (20 ka) conditions, the first experiment (ICE) involves only changing ice sheets and ocean bathymetry. Next, insolation forcing from changing orbital conditions was added (ICE+ORB). Then, greenhouse gases and (ICE+ORB+GHG) and meltwater fluxes were included (ICE+ORB+GHG+MWF). This allows approximate decomposition of the role of individual forcing factors through differencing pairs of experiments. Throughout this paper, I will refer to the first three experiments as ICE, ICE+ORB, and ICE+ORB+GHG. The experiment with all four forcing factors (ICE+ORB+GHG+MWF) represents the full iTraCE simulation and will be referred to as iTraCE, or without an explicit label when context is sufficiently clear. Further details about iTraCE are available in He et al. (2021a, 2021b).

I also utilize a fully coupled simulation using CESM1.2 as a preindustrial reference. Differences between CESM1.3 and CESM1.2 are minor, and involve a different gravity wave scheme and a few bug fixes in the radiative scheme (Meehl et al., 2019). CESM1.3 has been found to produce a preindustrial climate similar to CESM1.2 (Hurrell et al., 2013), so the preindindustrial CESM1.2 climate serves as a suitable control simulation. For model-data intercomparison, I use monthly-averaged precipitation and evaporation fields from the ERA-5 global reanalysis (Hersbach et al., 2020) over the period of 1979 to 2019.

3 Results

CESM reproduces realistic preindustrial precipitation minus evaporation ($P - E$) patterns (Figs. 2a, S3), and iTraCE produces wetter-than-modern conditions during the LGM (Fig. 2b). In contrast to TraCE-21ka, iTraCE shows robustly higher $P - E$ between 17 ka and 15 ka. iTraCE first shows a small decrease in $P - E$ over the western US at 18 ka (Fig. 2c), followed by a large increase at 16 ka along much of the California coast (Fig. 2d). Most of the western US is drier than at LGM at 14 ka (Fig. 2e), with a return to near-LGM conditions at 12 ka (Fig. 2f).

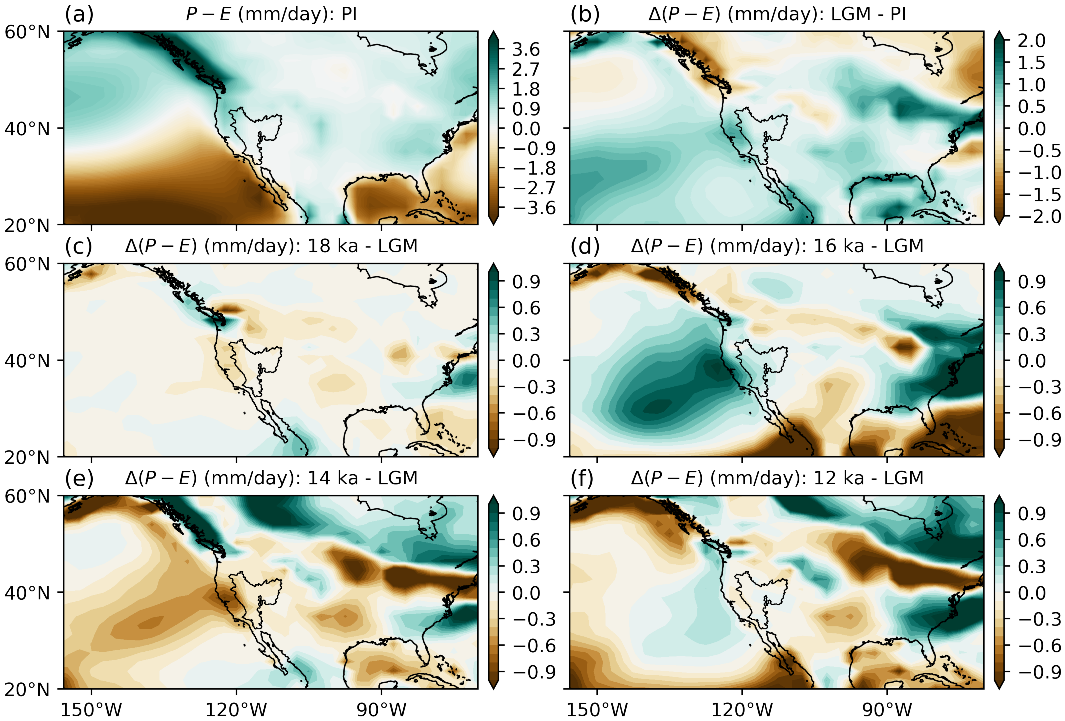

Figure 2. Maps of annual-mean $P - E$ in iTraCE. (a) $P - E$ in the preindustrial simulation. (b) Difference in $P - E$ between LGM (20 ka) and PI. (c) Difference between 18 ka and LGM. (d–f) As in (c), but for differences between 16, 14, and 12 ka from LGM respectively.

Figure 3 shows time series of annual-mean P and $P - E$ averaged over the Great Basin watershed. Precipitation decreases modestly from LGM to 18 ka, the start of Heinrich Stadial 1 (HS1; 18–14.7 ka). Precipitation then increases during HS1 until reaching a deglacial maximum around 16 ka that persists until 15 ka, the beginning of the Bølling-Allerød (14.7–13 ka). A rapid transition to dryer conditions is seen between 15 and 14 ka, and a modest increase in P is seen during the Younger Dryas (13–11.5 ka). Whereas TraCE-21ka shares some features with iTraCE, such as rapid drying of the Southwestern US during the Bølling-Allerød, the prominent peak in rainfall during HS1 seen here in both P and $P - E$ almost totally absent in TraCE-21ka. Fig. S4 shows the hydrological cycle for individual seasons and shows that changes in annual-mean P and $P - E$ are dominated by changes in winter rainfall.

Rainfall over the western US during the LGM is dominated by winter rain, and occurs in association with midlatitude cyclones and atmospheric rivers (Lora et al., 2017). The position and trajectories of storms are strongly influenced by the position of the midlatitude jet, and it is therefore useful to diagnose changes in the North Pacific jet (NPJ) over the course of deglaciation. I find that LGM state from iTraCE results in a south-

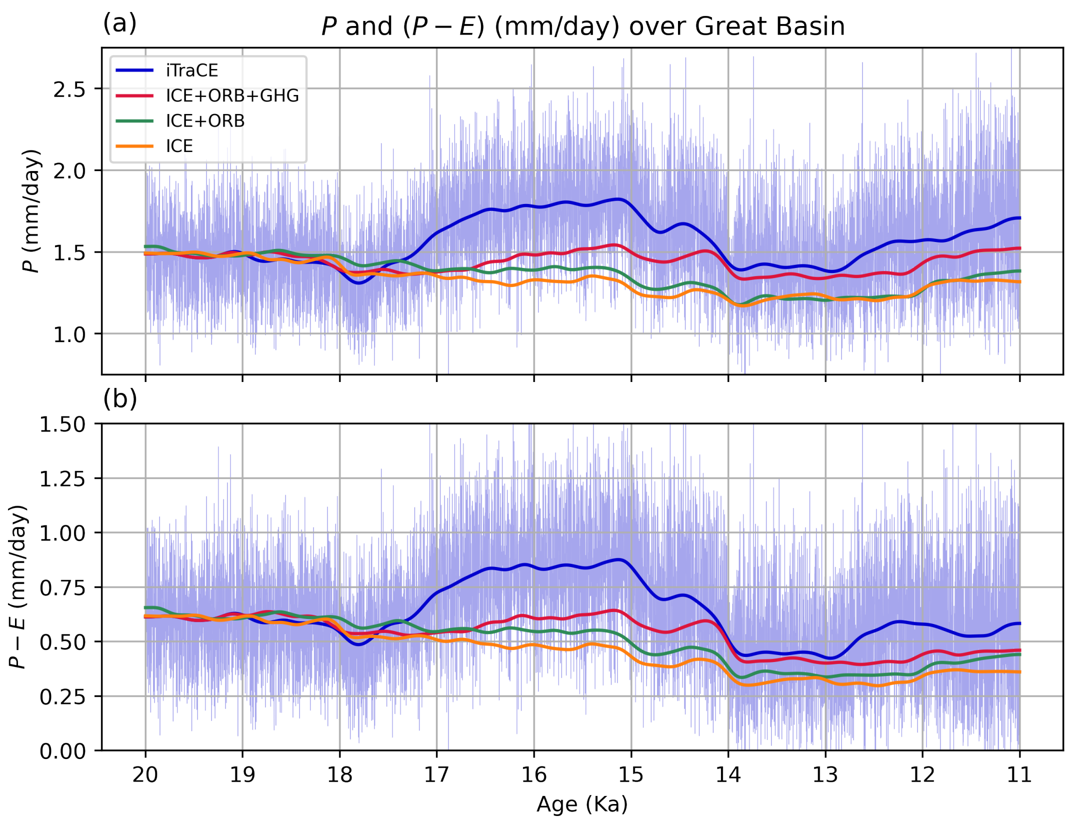

Figure 3. Hydrological cycle during deglaciation, averaged over the Great Basin watershed for experiments with four major forcing factors applied additively. (a) Annual-mean precipitation (P) from iTraCE, from 20 ka to 11 ka shown in the thin blue curve. The thick blue curve shows the long term trend for all experiments, with a Gaussian filter ($\sigma = 100$) applied. (b) As in panel (a), but for precipitation minus evaporation ($P - E$).

ward shift of the midlatitude jet compared to preindustrial, as shown by the difference in zonal velocity at 500 hPa (U500) between LGM and PI (Fig. 4b). This southward shift has been attributed to a PDO-like SST pattern induced by air-sea fluxes (Amaya et al., 2022).

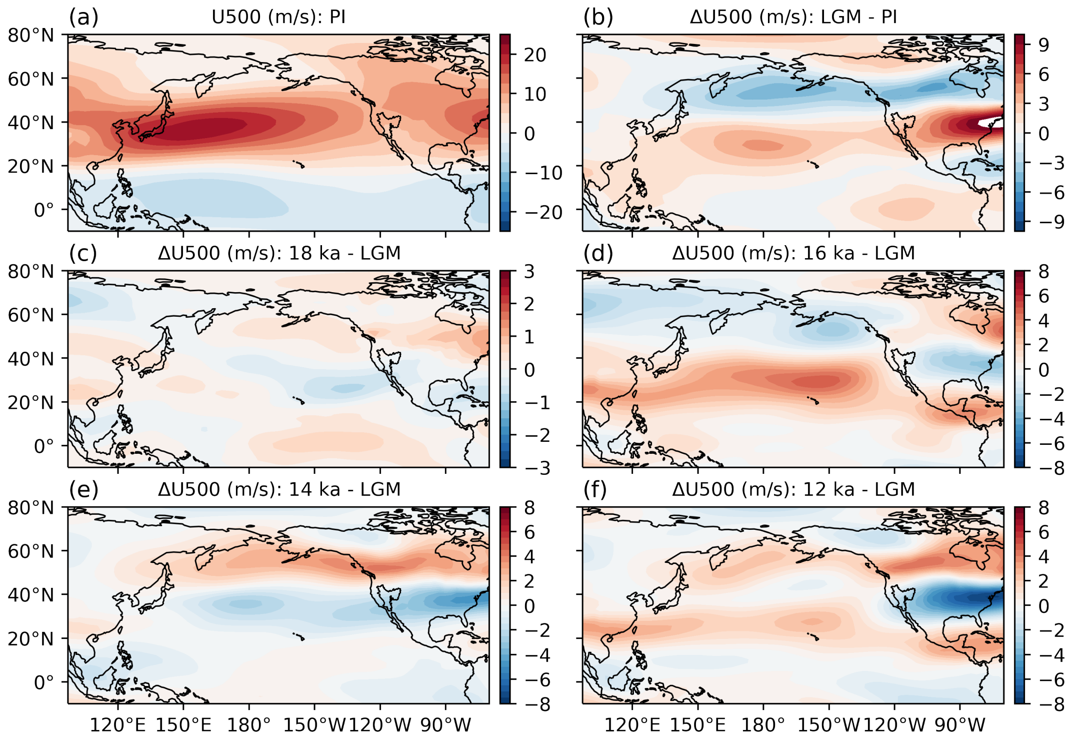

Figure 4. Annual-mean atmospheric circulation over the North Pacific. (a) Zonal velocity at 500 hPa (U500; m/s) in the preindustrial simulation. (b) Difference in U500 between LGM (20 ka) and PI. (c) Difference between 18 ka and LGM. (d–g) As in (c), but for differences between 16, 14, and 12 ka from LGM respectively.

At 18 ka, a slight northward shift of the NPJ is seen compared to LGM, with weakening zonal winds south of 40 °N and strengthening winds to the north (Fig. 4c). However, at 16 ka, a dramatic southward shift occurs, leading to increased winter rainfall associated with the position of extratropical storms (Fig. 4d). At 14 ka, the NPJ again migrates northwards, consistent with rapid drying of southwestern North America seen during the Bølling-Allerød (Fig. 4e). Differences between 12 ka conditions and LGM are more ambiguous, with some acceleration seen both both the subtropical and sub-polar latitudes over the North Pacific basin (Fig. 4f).

I now examine the most prominent feature of the hydrological cycle over the southwestern US during the last deglaciation: the inference of lake expansions and generally wetter conditions during HS1. Given that iTraCE reproduces wetter conditions at HS1 that compare favorably to proxy evidence, I quantify the contribution of various forcing factors. As mentioned in the methods section, iTraCE uses a "stacked forcing" approach that adds major forcing agents additively. I plot the long term trend in P and $P - E$ in these experiments in Fig. 3. The large difference between the full simulation (iTraCE; ICE+ORB+GHG+MWF) and the simulation excluding meltwater forcing (ICE+ORB+GHG) indicates that meltwater forcing plays a principal role in explaining lake expansions, leading to an increase in $P - E$ on the order of 0.20 mm/day between 20 ka and 16 ka. This is consistent with the findings of McGee et al. (2018), who used experiments to highlight the role of HS1 meltwater flux, albeit idealized orbital and ice sheet boundary conditions inconsistent with HS1.

However, closer examination of the ICE and ICE+ORB experiments reveals that the contribution of insolation and greenhouse gas forcing to western US lake expansions are non-negligible, with changing orbit and GHGs leading to a combined contribution of 0.14 mm/day $P-E$. In the absence of all major forcing factors besides waning ice sheets (ICE), nearly monotonic drying is seen between LGM and 13 ka (orange curve). Indeed, if wetter LGM conditions were primarily caused by the presence of North American ice sheets, then the waning of ice sheets must lead to drier conditions over the western US compared to LGM. The ICE+ORB+GHG experiment shows that changing insolation forcing and rising atmospheric CO_2 concentration lead to wetting of the western US that roughly cancels the drying from ice-sheet retreat. This suggests that meltwater forcing alone, in the absence of GHG and orbital forcing, may not have been sufficient to explain observed lake expansions during HS1. Timeseries for stacked forcing experiments for individual seasons are shown in Fig. S5.

Using the "stacked forcing" experiments, I approximately linear decompose the differences between 16 ka and LGM into individual forcing factors. 16 ka - LGM = (16 ka - 16 ka_ICE+ORB+GHG) + (16 ka_ICE+ORB+GHG - 16 ka_ICE+ORB) + (16 ka_ICE+ORB - 16 ka_ICE) + (16 ka_ICE - LGM). The four terms on the right hand side represent contributions from meltwater flux, greenhouse gases, changing, orbital conditions, and changing ice sheet boundary conditions. Maps of differences in $P-E$ linear separated are also shown in Fig. S6 and agree with Fig. 3. Using this method, I also decompose the contributions to the North Pacific atmospheric circulation into its individual components. Meltwater flux is found to lead to a dramatic southward shift of the midlatitude jet (Fig. 5a), consistent with the midlatitude response to a southward shift of the ITCZ during HS1 (McGee et al., 2014).

Rising greenhouse gases also lead to a southward shift of the jet (Fig. 5b), which is in contrast to inferences of poleward shift under future warming scenarios. The response of the midlatitude jet to GHG forcing is complex, involving the competing influences of increasing stratification, which tends to shift the jet polewards, and weakening meridional SST gradients caused by arctic warming, which tends to shift the jet equatorwards (Shaw et al., 2016; Matsumura et al., 2019). Furthermore, responses of the zonal-mean circulation to CO_2 forcing are less robust in the northern hemisphere and changes are not zonally symmetric (Simpson et al., 2014). Therefore, the equatorward shift seen here, although an interesting feature, it is not entirely unexpected given the significantly different reference state of the LGM climate compared to preindustrial. Figure 5c shows that changing orbital conditions further shift the jet southward, whereas a poleward shift occurs when only ice sheets change between LGM and 16 ka (Fig. 5d). Transects of U averaged between 120°W and 150°W are shown in Fig. S7.

Large-scale differences in surface temperature between 16 ka and LGM can help us better understand the atmospheric response. As can be seen in Fig. S8b, 16 ka conditions are characterized by a bipolar see-saw, with cooling in the northern hemisphere and warming in the southern hemisphere. This is primarily driven by North Atlantic meltwater fluxes, as shown by the contribution of this forcing factor (Fig. S8c). Closer examination of GHG forcing reveals a pattern of polar-amplified warming, a common feature of the surface temperature response to greenhouse gas forcing (Fig. S8d). This warming is particularly prominent in the North Atlantic as well as the the western North Pacific, as well as south of 50°S over the southern ocean.

Orbital forcing is found to lead to modest cooling in the low latitudes but warming at high latitudes particular in the northern hemisphere north of $\sim 40°$N (Figs. 6,S8e). This can be understood primarily as a response to increasing orbital obliquity between 20 ka and 16 ka (Berger & Loutre, 1991). The LGM was characterized by a moderate

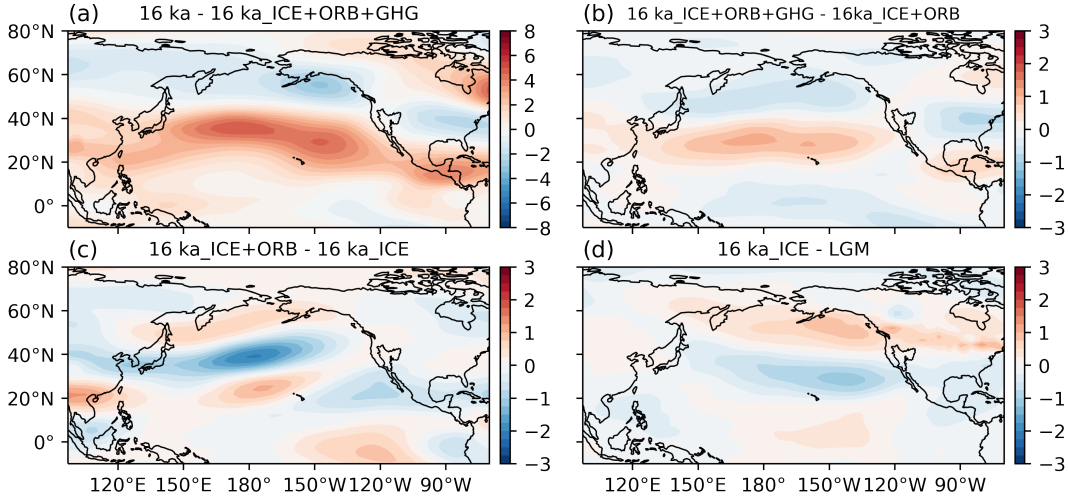

Figure 5. Difference in annual-mean atmospheric circulation between 16 ka and LGM, decomposed into contributions from various forcing factors. (a) Difference in zonal velocity at 500 hPa (U500; m/s) from meltwater forcing (16 ka - 16 ka_ICE+ORB+GHG). (b) Difference from greenhouse gas forcing (16 ka_ICE+ORB+GHG - 16 ka_ICE+ORB). (c) Difference from insolation forcing (16 ka_ICE+ORB - 16 ka_ICE). (d) Difference from changing ice sheets and bathymetry (16 ka_ice - LGM).

value of axial tilt (23.13°), whereas 16 ka was characterized by a relatively high obliquity of 23.76°. This leads to increased insolation north of 45°N and reduced insolation to the south of this latitude (Fig. S9), which helps explain the large-scale SST differences seen in (Figs. 6,S8).

A plot of differences in zonal-mean surface temperature is shown in Fig. 6. It is evident that meltwater forcing leads to a bipolar see-saw associated with strengthened meridional surface temperature gradients in the northern hemisphere midlatitudes, contributing to a strengthening of the North Pacific jet seen during HS1 (Fig. 5). Orbital and greenhouse gas forcing lead to strongly polar amplified warming, that reduces meridional SST gradients on the poleward flank of the NPJ, both contributing to a deceleration of the jet north of around 40 °N (Fig. 5b,c).

4 Discussion and Conclusions

In this study, I used iTraCE, a transient simulation of the deglaciation to study the evolution of western US hydroclimate during the last deglaciation. iTraCE compares favorably to evidence of lake expansions over western North America during the last deglaciation, producing increases in rainfall around Heinrich Stadial 1 that compare well to proxy evidence. Changes in rainfall are shown to result principally from meltwater forcing from Heinrich Stadial 1, with changes in orbital forcing and GHG concentrations playing a smaller, but non-negligible role in sustaining wetter conditions. Wetter conditions during HS1 are associated with a southward shift of the North Pacific jet, leading to transiently increasing winter rainfall over the Great Basin. This increased rainfall leads to a ∼20% increase in annual mean rainfall and ∼36% increase in annual-average $P - E$ over the Great Basin from LGM to 16 ka. After around 15 ka, the North American ice sheets retreat rapidly and the jet shifts northwards towards its modern configuration.

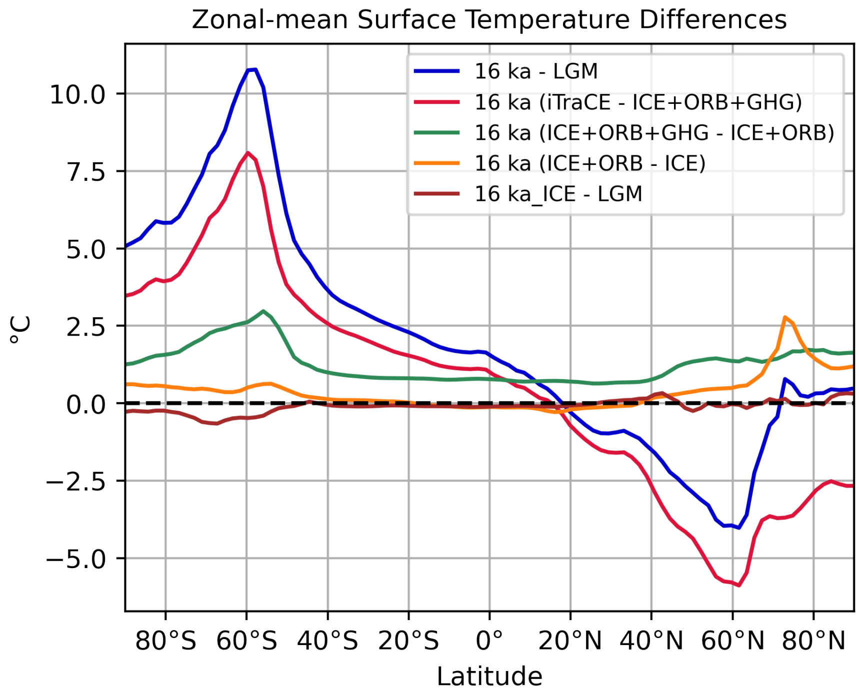

Figure 6. Zonal-mean and annual-mean surface temperature differences between 16 ka and LGM, linearly decomposed using additive forcing experiments.

While the 36% increase in $P-E$ that I identified falls short of fully explaining the magnitude of lake expansions during the last deglaciation, which ranged from 49% to 82% compared to LGM (McGee et al., 2018), it represents a notable improvement over previous modeling studies. It is possible that lake and vegetation feedbacks, which are absent in iTraCE due to the prescribed nature of land types, may act to further amplify the $P-E$ anomalies I identified (e.g., Hostetler et al., 1994). It is also possible that the iTraCE reproduces the correct magnitude and large-scale patterns of $P-E$ change, but small errors in the alignment of these large-scale patterns with the relatively small Great Basin domain could explain why they do not perfectly match proxy records. For instance, $P-E$ increases at HS1 are largest along the coast, so minute horizontal offsets in the Great Basin's position relative to the model grid could change the observed signal.

Another caveat of the approach employed in this study is that the decomposition of the forced responses works insofar as they can be considered to be linear forcings. McGee et al. (2018) showed the climate response to hosing experiments under varied orbital conditions could be quite different, so if the forcing factors in iTraCE were applied in a different order, the results could also differ somewhat. Therefore, although I have quantified the contributions of meltwater forcing, orbit, and greenhouse gases to western US hydroclimate during the last deglaciation, the precise magnitude of these contributions should ultimately be taken as approximate.

There are several possible reasons why the results of this study differ from those using TraCE-21ka, an earlier transient simulation that did not reproduce wetter conditions at HS1 compared to LGM. Major differences between TraCE-21ka and iTraCE include model version, horizontal resolution, as well as ice sheet boundary conditions. Indeed, ice-sheet reconstructions are highly uncertain (Gowan et al., 2021), so different reconstructions and histories of retreat could have large implications for the position of the midlatitude storm track and rainfall response (Ullman et al., 2014). Although the ice sheet boundary condition seems to be the most significant difference in boundary conditions between iTraCE and TraCE-21ka, the role of increased horizontal resolution and model version may also contribute to iTraCE's improved simulation of western US climate during deglaciation and should examined more closely in future studies.

Open Research

All post-processing scripts will be uploaded to a publicly available depository upon acceptance. iTraCE output is freely available at `https://doi.org/10.26024/b290-an76`.

Acknowledgments

I acknowledge Peter Molnar, Eli Tziperman, Jerry Mitrovica, Jiang Zhu, Tamara Pico, Mark Baum, Peter Huybers, and Jim Russell for helpful comments and discussions. I thank Bette Otto-Bliesner, Esther Brady, Robert Tomas, Zhengyu Liu, and Chengfei He, who produced iTraCE. This research was supported by the NSF Climate Dynamics program (joint NSF/NERC) grant AGS-1924538 and the Flint Postdoctoral Fellowship at Yale. I would like to acknowledge high-performance computing support from Cheyenne (doi:10.5065/D6RX99HX) provided by NCAR's Computational and Information Systems Laboratory, sponsored by the National Science Foundation. Additionally, comments from two anonymous reviewers improved the manuscript.

References

Adams, K. D., & Wesnousky, S. G. (1998). Shoreline processes and the age of the Lake Lahontan highstand in the Jessup embayment, Nevada. *Geological Society of America Bulletin*, *110*(10), 1318–1332.

Amaya, D. J., Seltzer, A. M., Karnauskas, K. B., Lora, J. M., Zhang, X., & DiNezio, P. N. (2022). Air-sea coupling shapes North American hydroclimate response to ice sheets during the Last Glacial Maximum. *Earth and Planetary Science Letters*, *578*, 117271.

Benson, L. V., Lund, S. P., Burdett, J. W., Kashgarian, M., Rose, T. P., Smoot, J. P., & Schwartz, M. (1998). Correlation of late-Pleistocene lake-level oscillations in Mono Lake, California, with North Atlantic climate events. *Quaternary Research*, *49*(1), 1–10.

Berger, A., & Loutre, M. F. (1991). Insolation values for the climate of the last 10 million years. *Quat. Sci. Rev.*, *10*, 297-317.

Bhattacharya, T., Tierney, J. E., & DiNezio, P. (2017). Glacial reduction of the North American Monsoon via surface cooling and atmospheric ventilation. *Geophysical Research Letters*, *44*(10), 5113–5122.

Brady, E. C., Otto-Bliesner, B. L., Kay, J. E., & Rosenbloom, N. (2013). Sensitivity to glacial forcing in the CCSM4. *Journal of Climate*, *26*(6), 1901–1925.

Brady, E. C., Stevenson, S., Bailey, D., Liu, Z., Noone, D., Nusbaumer, J., ... others (2019). The connected isotopic water cycle in the community earth system model version 1. *Journal of Advances in Modeling Earth Systems*, *11*(8), 2547–2566.

Broecker, W. S., & Orr, P. C. (1958). Radiocarbon chronology of Lake Lahontan and Lake Bonneville. *Geological Society of America Bulletin*, *69*(8), 1009–1032.

COHMAP Members. (1988). Climatic changes of the last 18,000 years: observations and model simulations. *Science*, *241*(4869), 1043–1052.

García, A. F., & Stokes, M. (2006). Late Pleistocene highstand and recession of a small, high-altitude pluvial lake, Jakes Valley, central Great Basin, USA. *Quaternary Research*, *65*(1), 179–186.

Gowan, E. J., Zhang, X., Khosravi, S., Rovere, A., Stocchi, P., Hughes, A. L., ...

Lohmann, G. (2021). A new global ice sheet reconstruction for the past 80 000 years. *Nature communications*, *12*(1), 1–9.

He, C., Liu, Z., Otto-Bliesner, B., Brady, E., Zhu, C., Tomas, R., ... others (2021b). Hydroclimate footprint of pan-asian monsoon water isotope during the last deglaciation. *Science Advances*, *7*(4), eabe2611.

He, C., Liu, Z., Otto-Bliesner, B. L., Brady, E. C., Zhu, C., Tomas, R., ... Severinghaus, J. P. (2021a). Abrupt heinrich stadial 1 cooling missing in greenland oxygen isotopes. *Science advances*, *7*(25), eabh1007.

Hersbach, H., Bell, B., Berrisford, P., Hirahara, S., Horányi, A., Muñoz-Sabater, J., ... others (2020). The ERA5 global reanalysis. *Quarterly Journal of the Royal Meteorological Society*, *146*(730), 1999–2049.

Hostetler, S. W., & Benson, L. V. (1990). Paleoclimatic implications of the high stand of Lake Lahontan derived from models of evaporation and lake level. *Climate dynamics*, *4*(3), 207–217.

Hostetler, S. W., Giorgi, F., Bates, G. T., & Bartlein, P. J. (1994). Lake-atmosphere feedbacks associated with paleolakes Bonneville and Lahontan. *Science*, *263*(5147), 665–668.

Hudson, A. M., Quade, J., Ali, G., Boyle, D., Bassett, S., Huntington, K. W., ... Wang, X. (2017). Stable C, O and clumped isotope systematics and ^{14}c geochronology of carbonates from the Quaternary Chewaucan closed-basin lake system, Great Basin, USA: Implications for paleoenvironmental reconstructions using carbonates. *Geochimica et Cosmochimica Acta*, *212*, 274–302.

Hurrell, J. W., Holland, M. M., Gent, P. R., Ghan, S., Kay, J. E., Kushner, P. J., ... others (2013). The community earth system model: a framework for collaborative research. *Bulletin of the American Meteorological Society*, *94*(9), 1339–1360.

Ibarra, D. E., Egger, A. E., Weaver, K. L., Harris, C. R., & Maher, K. (2014). Rise and fall of late Pleistocene pluvial lakes in response to reduced evaporation and precipitation: Evidence from Lake Surprise, California. *Bulletin*, *126*(11-12), 1387–1415.

Ibarra, D. E., Oster, J. L., Winnick, M. J., Caves Rugenstein, J. K., Byrne, M. P., & Chamberlain, C. P. (2018). Warm and cold wet states in the western United States during the Pliocene–Pleistocene. *Geology*, *46*(4), 355–358.

Jayko, A. S., Forester, R. M., Kaufman, D. S., Phillips, F. M., Yount, J. C., McGeehin, J., & Mahan, S. A. (2008). Late Pleistocene lakes and wetlands, Panamint Valley, Inyo County, California. *Late Cenozoic Drainage History of the Southwestern Great Basin and Lower Colorado River Region: Geologic and Biotic Perspectives,* edited by M.C. Reheis, R. Hershler, and D.M. Miller*, The Geological Society of America Special Paper 439*, 151-184.

Kageyama, M., Harrison, S. P., Kapsch, M.-L., Lofverstrom, M., Lora, J. M., Mikolajewicz, U., ... others (2021). The pmip4 last glacial maximum experiments: preliminary results and comparison with the pmip3 simulations. *Climate of the Past*, *17*(3), 1065–1089.

Kutzbach, J. E., & Wright Jr, H. E. (1985). Simulation of the climate of 18,000 years BP: Results for the North American/North Atlantic/European sector and comparison with the geologic record of North America. *Quaternary Science Reviews*, *4*(3), 147–187.

Liu, Z., Otto-Bliesner, B. L., He, F., Brady, E. C., Tomas, R., Clark, P. U., ... Cheng, J. (2009). Transient simulation of last deglaciation with a new mechanism for Bølling-Allerød warming. *Science*, *325*(5938), 310–314.

Lofverstrom, M. (2020). A dynamic link between high-intensity precipitation events in southwestern north america and europe at the last glacial maximum. *Earth and Planetary Science Letters*, *534*, 116081.

Lora, J. M., & Ibarra, D. E. (2019). The North American hydrologic cycle through the last deglaciation. *Quaternary Science Reviews*, *226*, 105991.

Lora, J. M., Mitchell, J. L., Risi, C., & Tripati, A. E. (2017). North Pacific atmospheric rivers and their influence on western North America at the Last Glacial Maximum. *Geophysical Research Letters*, *44*(2), 1051–1059.

Lora, J. M., Mitchell, J. L., & Tripati, A. E. (2016). Abrupt reorganization of north pacific and western north american climate during the last deglaciation. *Geophysical Research Letters*, *43*(22), 11–796.

Lüthi, D., Le Floch, M., Bereiter, B., Blunier, T., Barnola, J.-M., Siegenthaler, U., … others (2008). High-resolution carbon dioxide concentration record 650,000–800,000 years before present. *nature*, *453*(7193), 379–382.

Lyle, M., Heusser, L., Ravelo, C., Yamamoto, M., Barron, J., Diffenbaugh, N. S., … Andreasen, D. (2012). Out of the tropics: the Pacific, Great Basin Lakes, and Late Pleistocene water cycle in the western United States. *Science*, *337*(6102), 1629–1633.

Manabe, S., & Broccoli, A. J. (1985). The influence of continental ice sheets on the climate of an ice age. *J. Geophys. Res.*, *90*, 2167–2190.

Matsumura, S., Ueki, S., & Horinouchi, T. (2019). Contrasting responses of midlatitude jets to the north pacific and north atlantic warming. *Geophysical research letters*, *46*(7), 3973–3981.

McGee, D., Donohoe, A., Marshall, J., & Ferreira, D. (2014). Changes in itcz location and cross-equatorial heat transport at the last glacial maximum, heinrich stadial 1, and the mid-holocene. *Earth and Planetary Science Letters*, *390*, 69–79.

McGee, D., Moreno-Chamarro, E., Marshall, J., & Galbraith, E. (2018). Western US lake expansions during Heinrich stadials linked to Pacific Hadley circulation. *Science advances*, *4*(11), eaav0118.

McGee, D., Quade, J., Edwards, R. L., Broecker, W. S., Cheng, H., Reiners, P. W., & Evenson, N. (2012). Lacustrine cave carbonates: Novel archives of paleohydrologic change in the Bonneville Basin (Utah, USA). *Earth and Planetary Science Letters*, *351*, 182–194.

Meehl, G. A., Yang, D., Arblaster, J. M., Bates, S. C., Rosenbloom, N., Neale, R., … others (2019). Effects of model resolution, physics, and coupling on southern hemisphere storm tracks in cesm1. 3. *Geophysical Research Letters*, *46*(21), 12408–12416.

Mifflin, M. D., & Wheat, M. M. (1979). *Pluvial lakes and estimated pluvial climates of nevada* (Vol. 94). Mackay School of Mines, University of Nevada.

Monnin, E., Indermuhle, A., Dallenbach, A., Fluckiger, J., Stauffer, B., Stocker, T. F., … Barnola, J.-M. (2001). Atmospheric CO_2 concentrations over the last glacial termination. *science*, *291*(5501), 112–114.

Munroe, J. S., & Laabs, B. J. C. (2013a). Latest Pleistocene history of pluvial Lake Franklin, northeastern Nevada, USA. *GSA Bulletin*, *125*(3-4), 322–342.

Munroe, J. S., & Laabs, B. J. C. (2013b). Temporal correspondence between pluvial lake highstands in the southwestern US and Heinrich Event 1. *Journal of Quaternary Science*, *28*(1), 49–58.

Oster, J. L., Ibarra, D. E., Winnick, M. J., & Maher, K. (2015). Steering of westerly storms over western North America at the Last Glacial Maximum. *Nature Geoscience*, *8*(3), 201–205.

Oviatt, C. G. (2015). Chronology of Lake Bonneville, 30,000 to 10,000 yr BP. *Quaternary Science Reviews*, *110*, 166–171.

Peltier, W. R. (2004). Global glacial isostasy and the surface of the ice-age Earth: the ICE-5G (VM2) model and GRACE. *Annu. Rev. Earth Planet. Sci.*, *32*, 111–149.

Peltier, W. R., Argus, D., & Drummond, R. (2015). Space geodesy constrains ice age terminal deglaciation: The global ice-6g_c (vm5a) model. *Journal of Geophysical Research: Solid Earth*, *120*(1), 450–487.

Reheis, M. C., Adams, K. D., Oviatt, C. G., & Bacon, S. N. (2014). Pluvial lakes in

the Great Basin of the western United States – A view from the outcrop. *Quaternary Science Reviews*, *97*, 33–57.
Scheff, J., Seager, R., Liu, H., & Coats, S. (2017). Are glacials dry? Consequences for paleoclimatology and for greenhouse warming. *Journal of Climate*, *30*(17), 6593–6609.
Shaw, T., Baldwin, M., Barnes, E. A., Caballero, R., Garfinkel, C., Hwang, Y.-T., ... others (2016). Storm track processes and the opposing influences of climate change. *Nature Geoscience*, *9*(9), 656–664.
Simpson, I. R., Shaw, T. A., & Seager, R. (2014). A diagnosis of the seasonally and longitudinally varying midlatitude circulation response to global warming. *Journal of the Atmospheric Sciences*, *71*(7), 2489–2515.
Tabor, C., Lofverstrom, M., Oster, J., Wortham, B., de Wet, C., Montañez, I., ... Liu, Z. (2021). A mechanistic understanding of oxygen isotopic changes in the western united states at the last glacial maximum. *Quaternary Science Reviews*, *274*, 107255.
Ullman, D. J., LeGrande, A. N., Carlson, A. E., Anslow, F. S., & Licciardi, J. M. (2014). Assessing the impact of Laurentide Ice Sheet topography on glacial climate. *Climate of the Past*, *10*(2), 487–507.

Figure1.

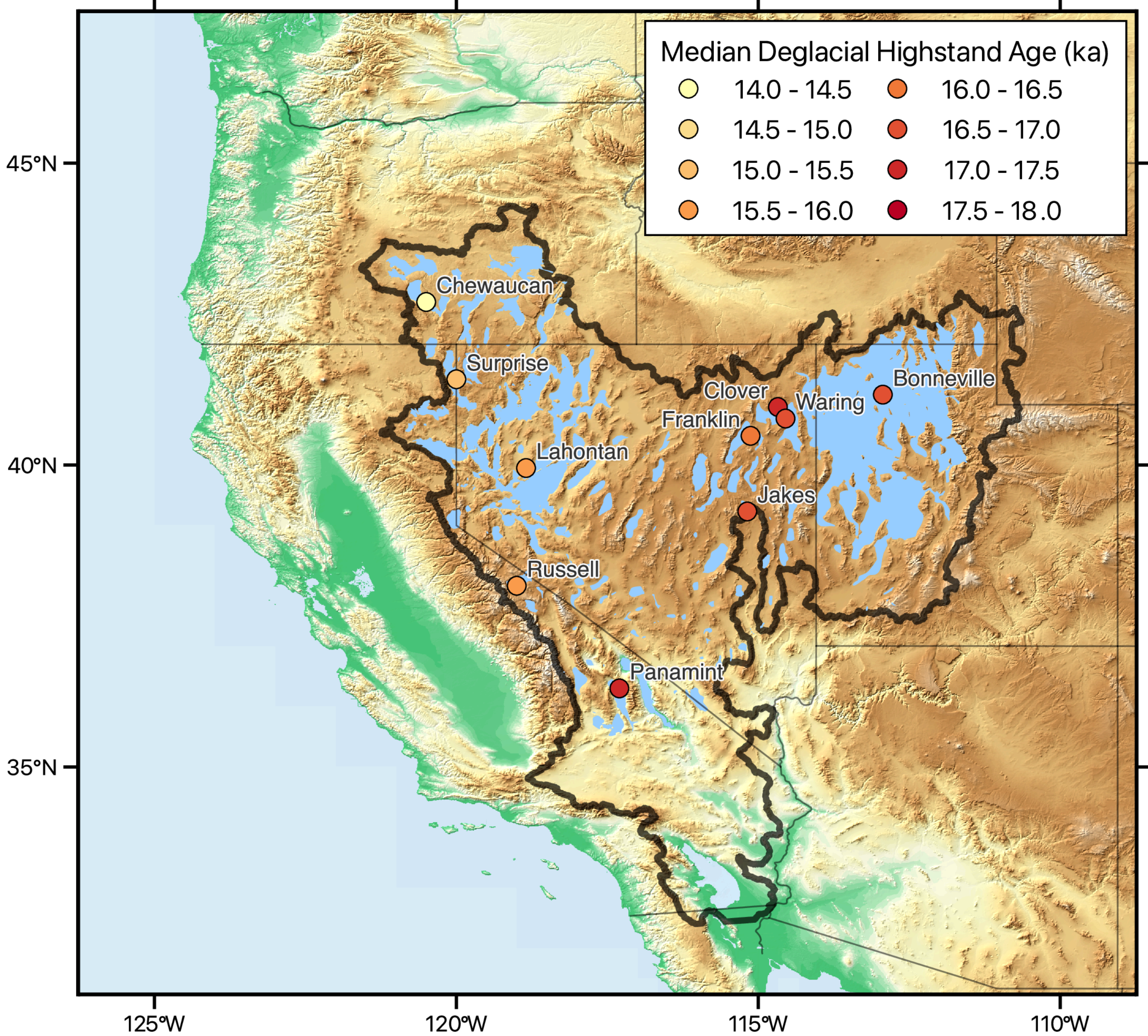

Median Deglacial Highstand Age (ka)
14.0 - 14.5
14.5 - 15.0
15.0 - 15.5
15.5 - 16.0
16.0 - 16.5
16.5 - 17.0
17.0 - 17.5
17.5 - 18.0
Chewaucan
Surprise
Lahontan
Russell
Panamint
Clover
Waring
Franklin
Jakes
Bonneville
45°N
40°N
35°N
125°W
120°W
115°W
110°W

Figure2.

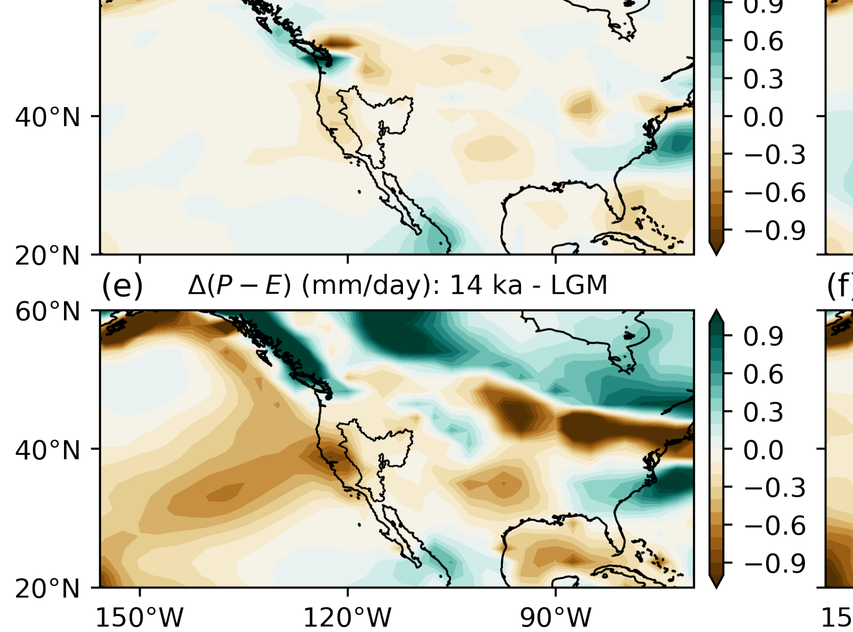

40°N
20°N
0.9
0.6
0.3
0.0
−0.3
−0.6
−0.9
(e)
Δ(P − E) (mm/day): 14 ka - LGM
60°N
40°N
20°N
0.9
0.6
0.3
0.0
−0.3
−0.6
−0.9
150°W
120°W
90°W
(f
15

Figure3.

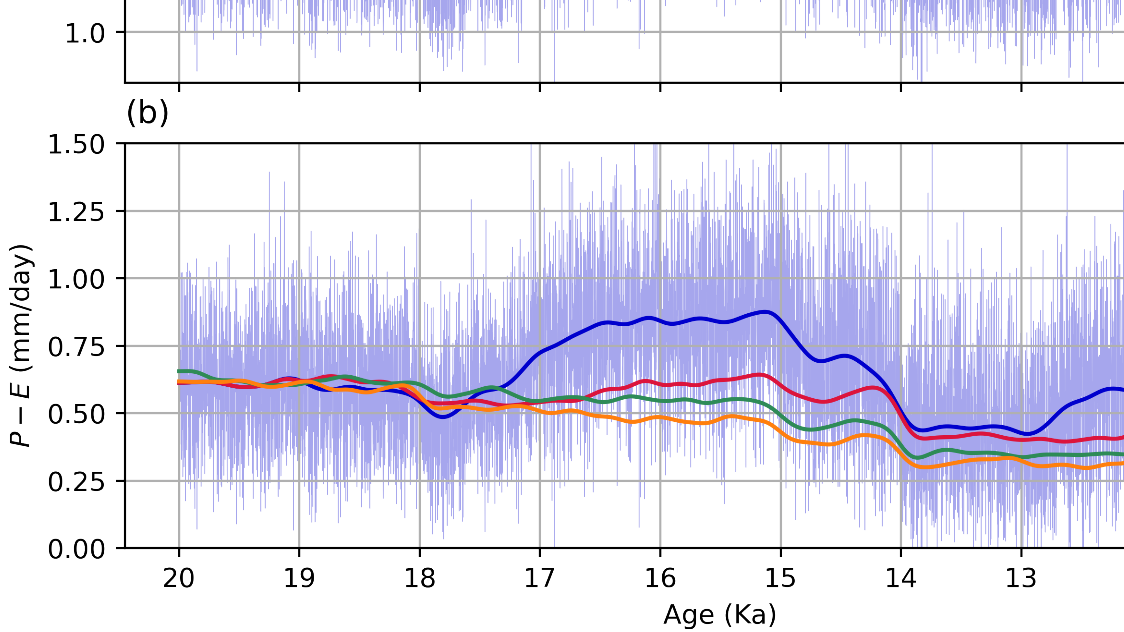
1.0
(b)
1.50
1.25
1.00
0.75
0.50
0.25
0.00
$P - E$ (mm/day)
20
19
18
17
16
15
14
13
Age (Ka)

Figure4.

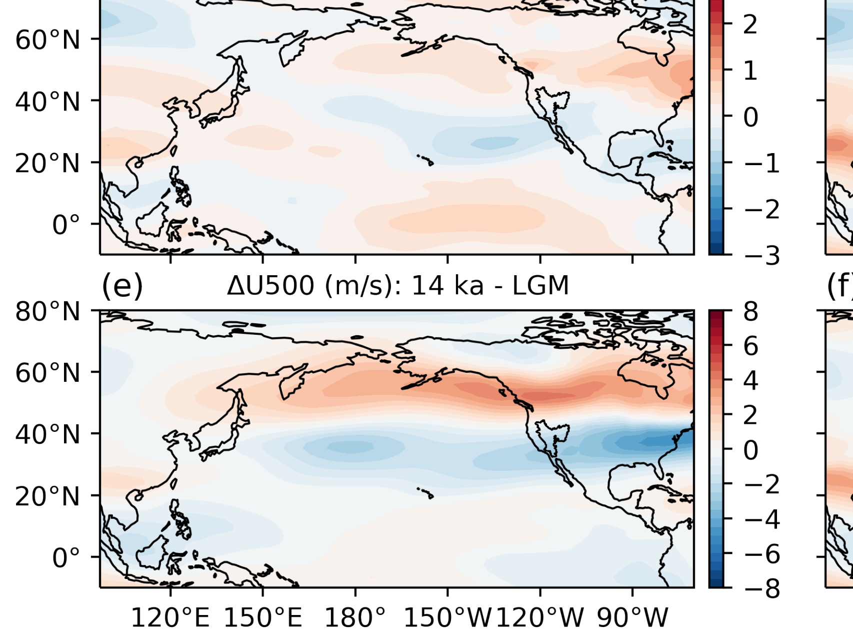

60°N
40°N
20°N
0°
2
1
0
−1
−2
−3
(e)
ΔU500 (m/s): 14 ka - LGM
80°N
60°N
40°N
20°N
0°
8
6
4
2
0
−2
−4
−6
−8
120°E
150°E
180°
150°W
120°W
90°W
(f)

Figure5.

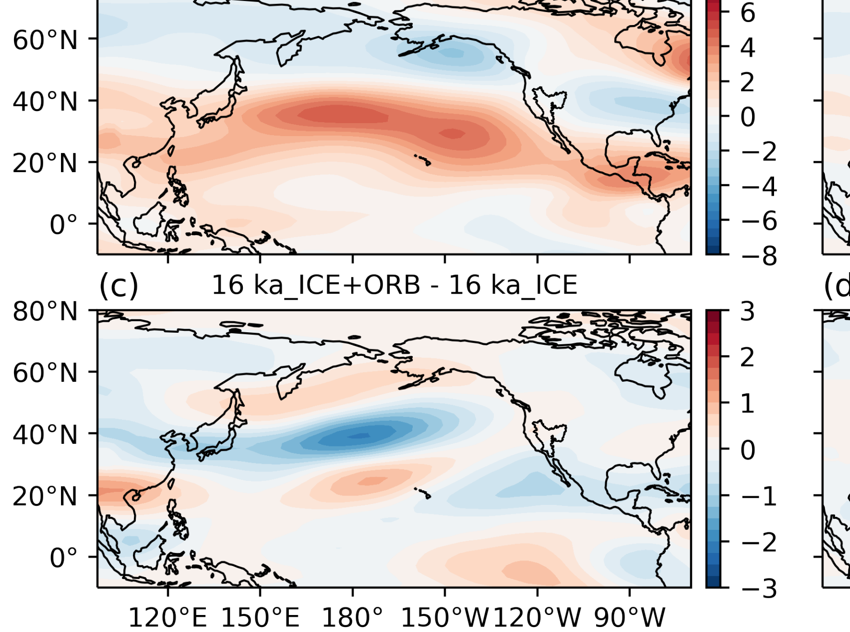
(c)
16 ka_ICE+ORB - 16 ka_ICE
(d
80°N
60°N
40°N
20°N
0°
120°E
150°E
180°
150°W
120°W
90°W
6
4
2
0
−2
−4
−6
−8
3
2
1
0
−1
−2
−3

Figure6.

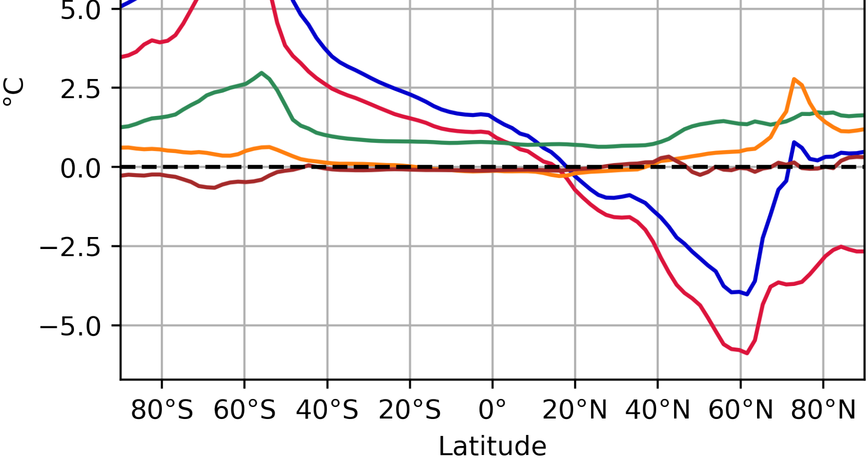
5.0
2.5
0.0
−2.5
−5.0
°C
80°S
60°S
40°S
20°S
0°
20°N
40°N
60°N
80°N
Latitude

Supporting Information for "Revisiting western United States hydroclimate during the last deglaciation"

Minmin Fu[1]

[1]Department of Earth and Planetary Sciences, Yale University, New Haven, CT, USA

Contents of this file

1. Figures S1 to S9

2. References

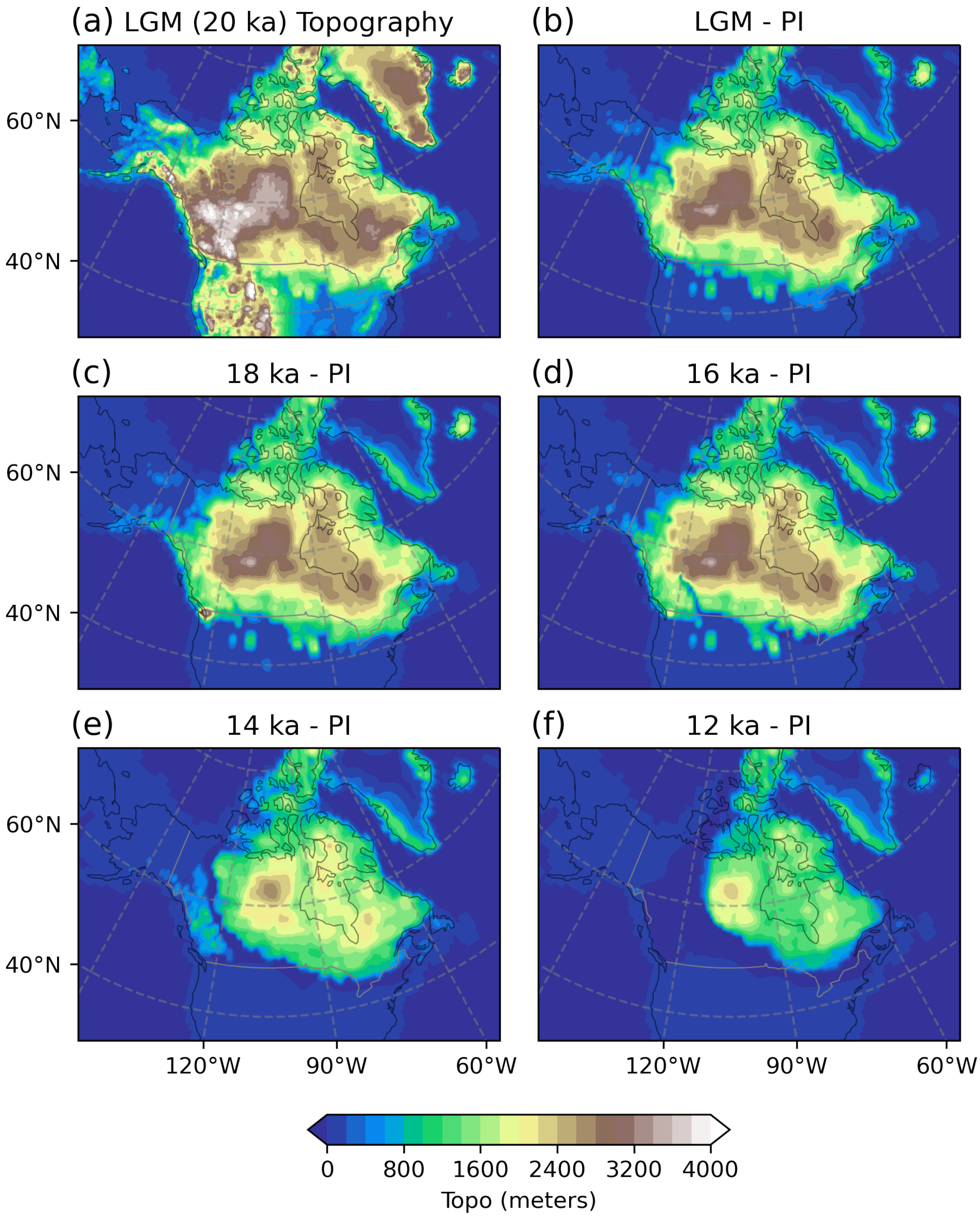

Figure S1. (a) Ice-sheet topography (meters) during the LGM (20 ka) from the ICE-6G reconstruction (Peltier et al., 2015). (b) Difference in ice-sheet topography between LGM and preindustrial. (c–f) As in (b), but differences from Preindustrial for 18, 16, 14, and 12 ka, respectively.

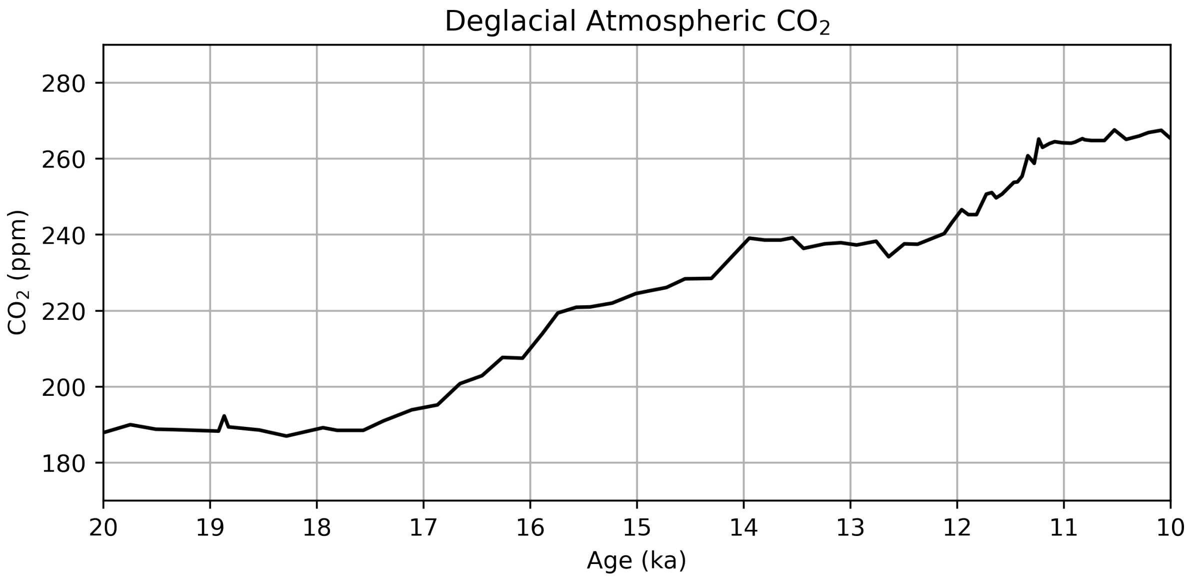

Figure S2. Atmospheric CO_2 concentration during the last deglaciation (Lüthi et al., 2008; Monnin et al., 2001).

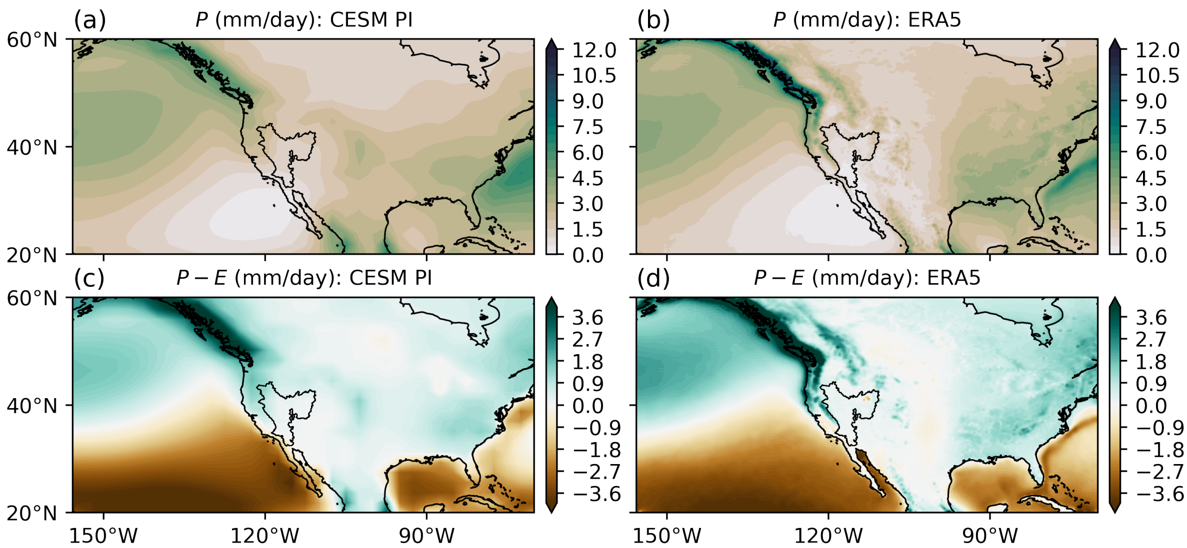

Figure S3. (a) Annual-mean precipitation rate for the preindustrial CESM simulation. (b) As in (a), but for ERA5 reanalysis. (c) Annual-mean precipitation minus evaporation ($P-E$) for preindustrial CESM. (d) As in (c), but for ERA5 reanalysis.

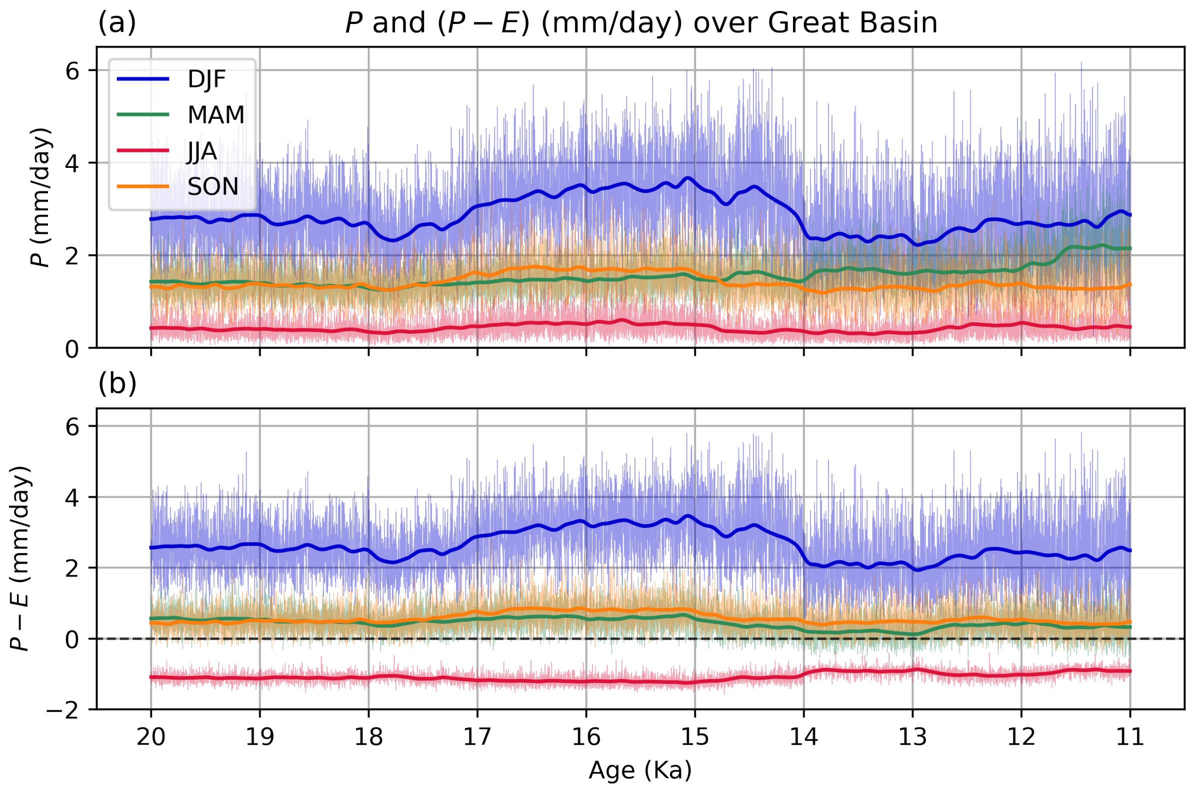

Figure S4. Hydrological cycle during deglaciation, averaged over the Great Basin watershed, for individual seasons. (a) Seasonal mean precipitation (P), from 20 ka to 11 ka shown in the thin curve. The thick curve shows the long term trend, with a Gaussian filter ($\sigma = 100$) applied. (b) As in panel (a), but for precipitation minus evaporation ($P - E$).

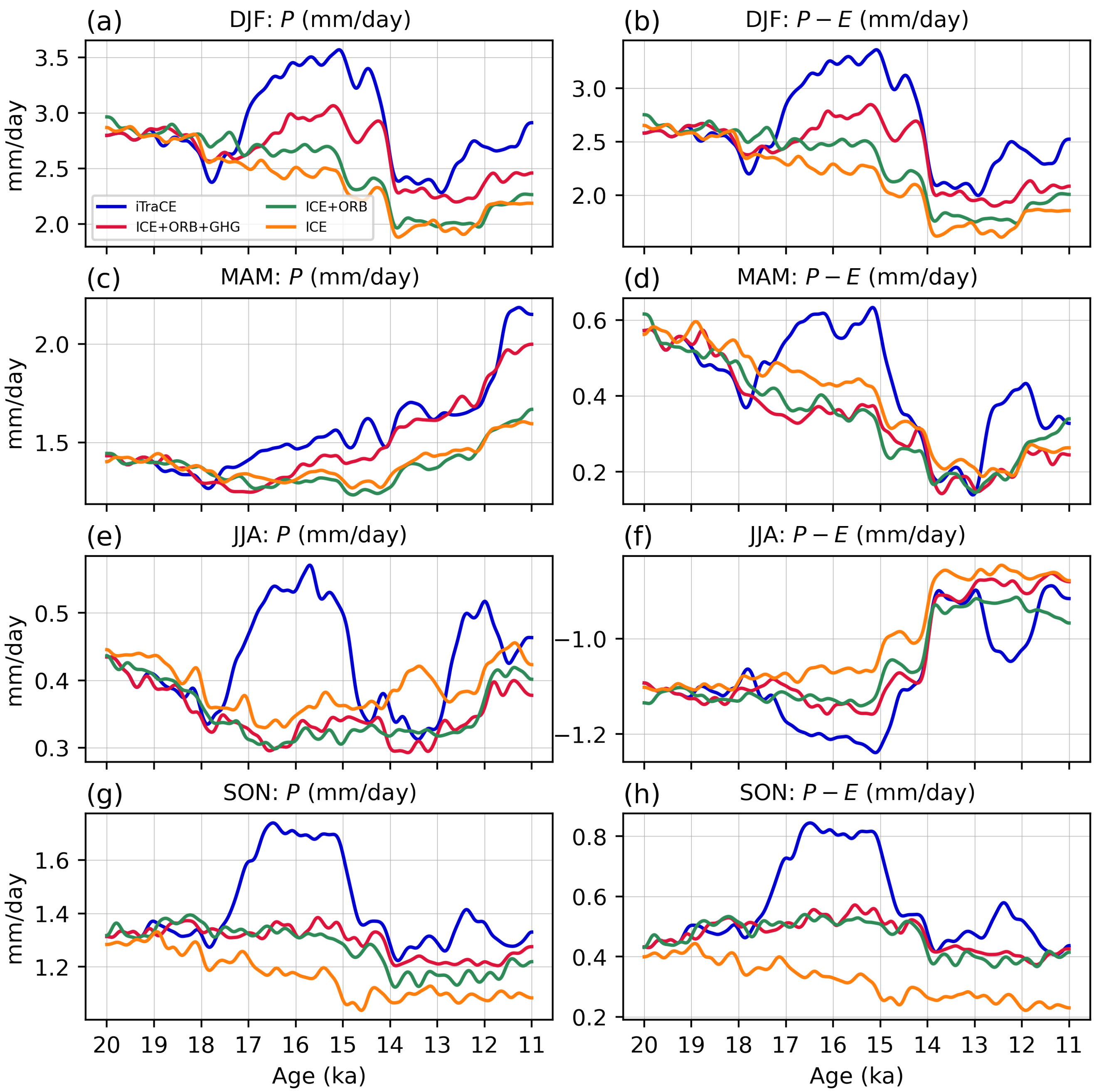

Figure S5. Hydrological cycle over the Great Basin watershed in additive forcing experiments, for individual seasons. (a) Long term trend in seasonal mean precipitation (P), from 20 ka to 11 ka, with four major forcing factors applied additively. A Gaussian filter ($\sigma = 100$) has been applied to all curves. (b) As in panel (a), but for precipitation minus evaporation ($P - E$). (c,d) As in (a,b), but for MAM. (e,f) As in (a,b), but for JJA. (g,h) As in (a,b), but for SON.

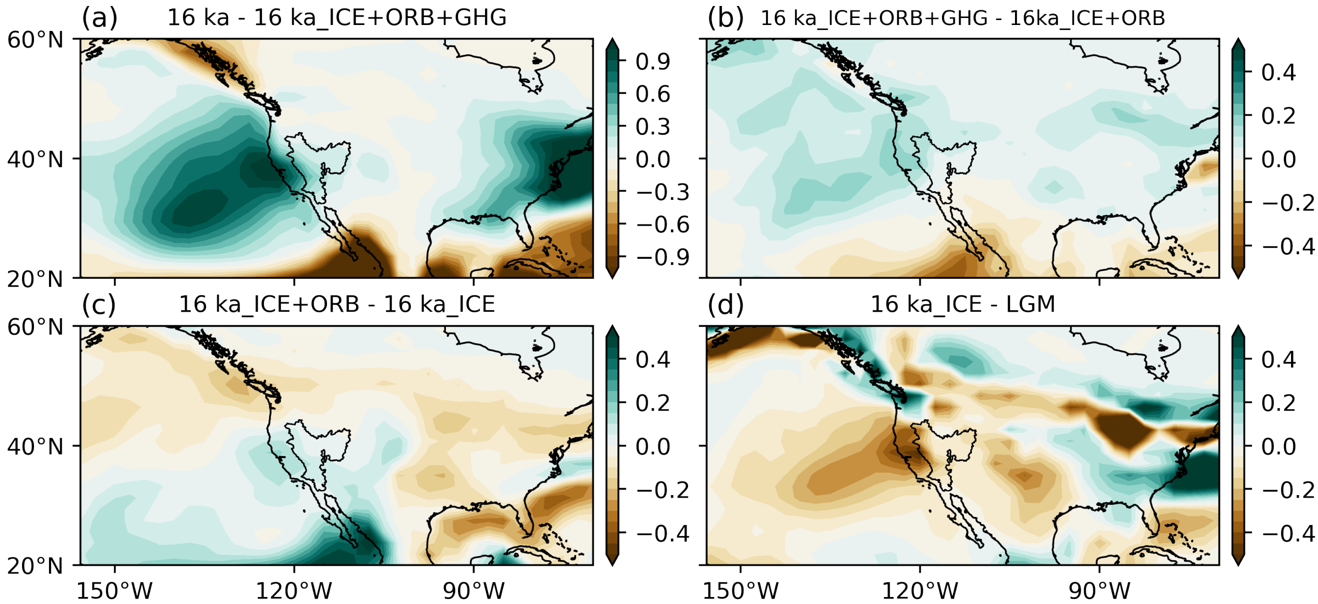

Figure S6. Difference in annual-mean $P - E$ between 16 ka and LGM, decomposed into contributions from various forcing factors. (a) Difference in $P - E$ from meltwater forcing (16 ka - 16 ka_ICE+ORB+GHG). (b) Difference from greenhouse gas forcing (16 ka_ICE+ORB+GHG - 16 ka_ICE+ORB). (c) Difference from insolation forcing (16 ka_ICE+ORB - 16 ka_ICE). (d) Difference from changing ice sheets and bathymetry (16 ka_ICE - LGM).

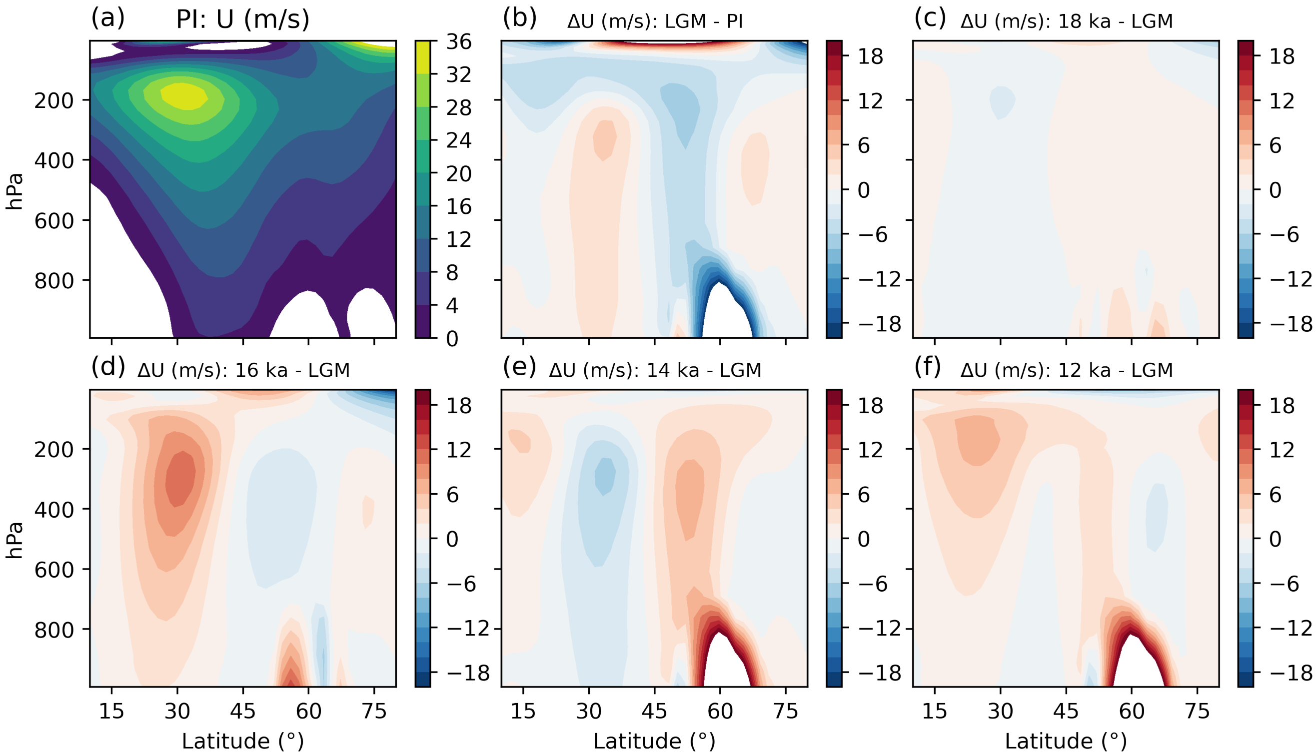

Figure S7. Annual-mean zonal winds averaged over the eastern North Pacific (120°W–150°W). (a) U (m/s) in the preindustrial simulation. (b) Difference between and LGM and PI. (c) Difference between 18 ka and LGM. (d–f) As in (c), but differences from LGM for 16 ka, 14 ka, and 12 ka, respectively.

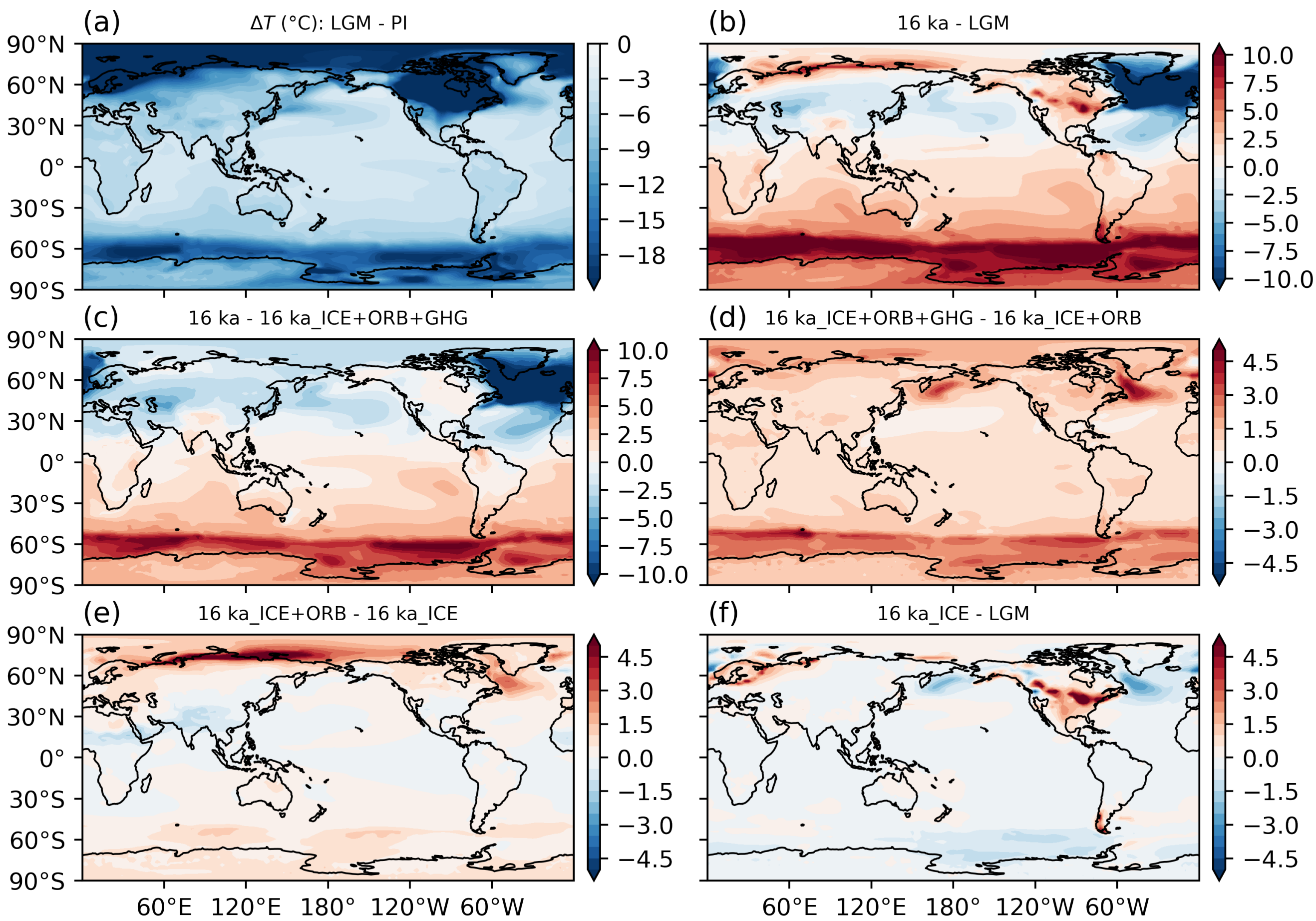

Figure S8. (a) Annual-mean surface temperature differences between LGM and PI. (b) Difference between 16 ka and LGM. (c) Difference in surface temperature from meltwater forcing (16 ka - 16 ka_ICE+ORB+GHG). (d) Difference from greenhouse gas forcing (16 ka_ICE+ORB+GHG - 16 ka_ICE+ORB). (e) Difference from insolation forcing (16 ka_ICE+ORB - 16 ka_ICE). (f) Difference from changing ice sheets and bathymetry (16 ka_ICE - LGM).

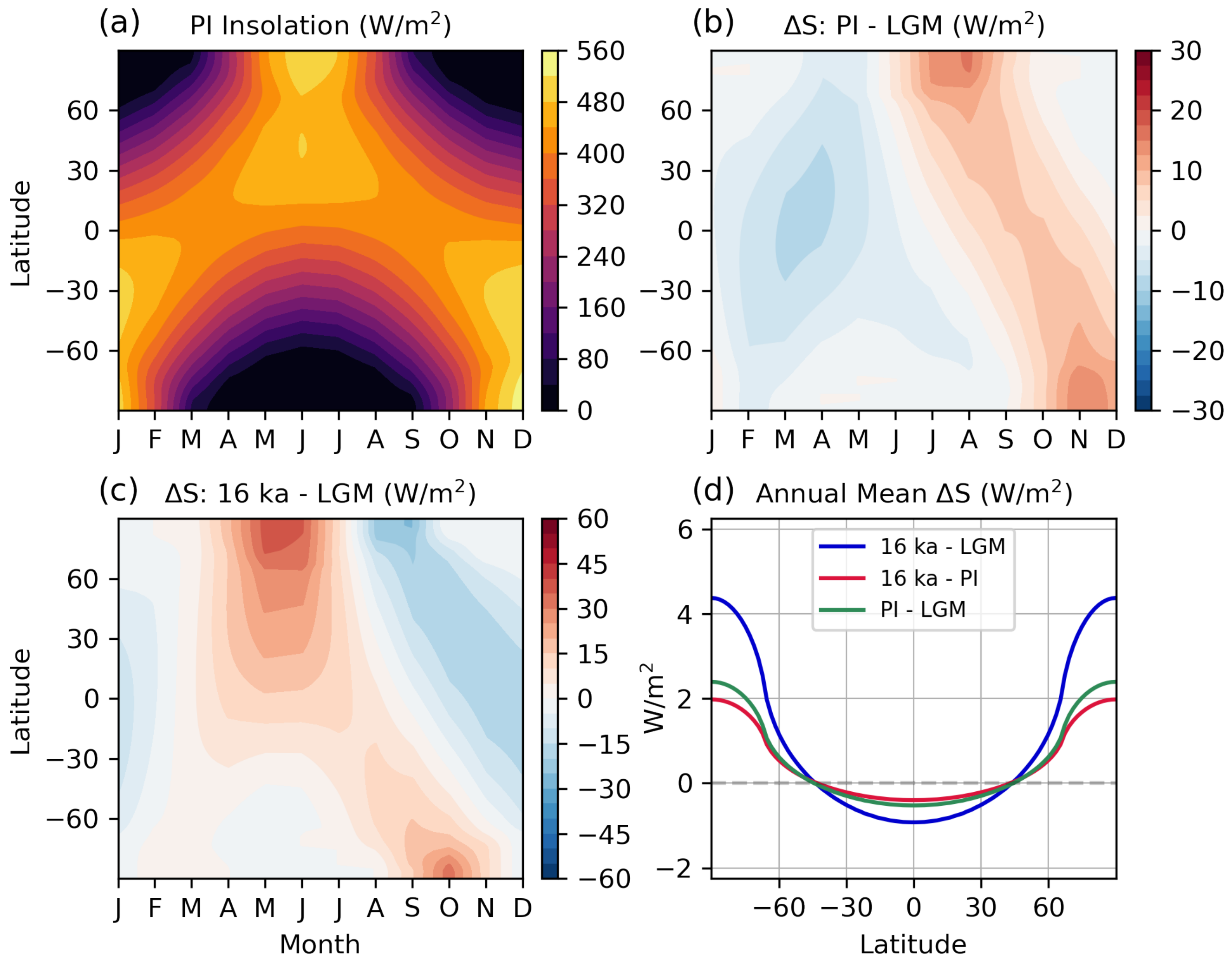

Figure S9. (a) Insolation as a function of season and latitude in the preindustrial simulation. (b) Difference in insolation between PI and LGM. (c) As in (b), but for the difference between 16 ka and LGM. (d) Zonal-mean insolation differences between 16 ka and LGM, 16 ka and PI, and PI and LGM, reflecting differences in obliquity. Vernal equinox is defined as March 21st at noon for all experiments.

References

Lüthi, D., Le Floch, M., Bereiter, B., Blunier, T., Barnola, J.-M., Siegenthaler, U., ... others (2008). High-resolution carbon dioxide concentration record 650,000–800,000 years before present. *nature*, *453*(7193), 379–382.

Monnin, E., Indermuhle, A., Dallenbach, A., Fluckiger, J., Stauffer, B., Stocker, T. F., ... Barnola, J.-M. (2001). Atmospheric CO_2 concentrations over the last glacial termination. *science*, *291*(5501), 112–114.

Peltier, W. R., Argus, D., & Drummond, R. (2015). Space geodesy constrains ice age terminal deglaciation: The global ice-6g_c (vm5a) model. *Journal of Geophysical Research: Solid Earth*, *120*(1), 450–487.